Strange Nonchaotic Bursting in a Quasiperiodically-forced Hindmarsh-Rose Neuron

Woochang Lim* and Sang-Yoon Kim†

Department of Physics, Kangwon National University, Chunchon 200-701

(Received 14 October 2010)

We study the transition from a silent state to a bursting state by varying the dc stimulus in the Hindmarsh-Rose neuron under quasiperiodic stimulation. For this quasiperiodically-forced case, a new type of strange nonchaotic (SN) bursting state is found to occur between the silent state and the chaotic bursting state. This is in contrast to the periodically-forced case where the silent state transforms directly to a chaotic bursting state. Using a rational approximation to the quasiperiodic forcing, we investigate the mechanism for the appearance of such an SN bursting state. Thus, a smooth torus (corresponding to a silent state) is found to transform to an SN bursting attractor through a phase-dependent subcritical period-doubling bifurcation. These SN bursting states, together with chaotic bursting states, are characterized in terms of the interburst interval, the bursting length, and the number of spikes in each burst. Both bursting states are found to be aperiodic complex ones. Consequently, aperiodic complex burstings may result from two dynamically different states with strange geometry (one is chaotic and the other is nonchaotic). Thus, in addition to chaotic burstings, SN burstings may become a dynamical origin for the complex physiological rhythms that are ubiquitous in organisms.

I. INTRODUCTION

To probe the dynamical properties of a system, one often applies an external stimulus to the system and study its response. Particularly, periodic stimulation of biological oscillators has attracted much attention in various systems such as the embryonic chick heart-cell aggregates [1], squid giant axons [2,3], and cortical pyramidal neurons [4]. Rich regular (such as phase locking and quasiperiodicity) and chaotic responses were found in these periodically forced systems [5,6]. In contrast, the quasiperiodically-forced case has received little attention [7,8]; hence, further intensive investigation on the dynamical responses of quasiperiodically-forced biological oscillators is necessary.

Here, we are interested in neural bursting activity [alternating between a silent phase and an active (bursting) phase of repetitive spikings] [9]. Cortical intrinsically bursting neurons, thalamocortical relay neurons, thalamic reticular neurons, and hippocampal pyramidal neurons are representative examples of bursting neurons [10]. We are particularly concerned with dynamical responses of bursting neurons subject to quasiperiodic

stimulation. Strange nonchaotic (SN) attractors typically appear in quasiperiodically-forced dynamical systems [11–14]. They exhibit some properties of regular, as well as chaotic, attractors. Like regular attractors, their dynamics is nonchaotic in the sense that they do not have a positive Lyapunov exponent; like usual chaotic attractors, they have a geometrically strange (fractal) structure. Hence, SN burstings are expected to occur in quasiperiodically-forced bursting neurons.

This paper is organized as follows. In Sec. II., we consider the Hindmarsh-Rose (HR) neuron model for bursting neurons, which was originally introduced to describe the time evolution of the membrane potential for the pond snail [9,15,16], and investigate the transition from a silent state to a bursting state by varying the dc stimulus. This work on bursting neurons is in contrast to previous works on spiking neurons [8]. In the periodically-forced case (*i.e.*, in the presence of only one ac stimulus source), an intermittent transition from a silent state (with subthreshold oscillations) to a chaotic bursting state occurs when the dc stimulus passes a threshold value. The effect of the quasiperiodic forcing on this intermittent route to chaotic bursting is investigated by adding another independent ac stimulus source. Thus, unlike the case of a periodic stimulus, new types of SN burstings are found to occur as intermediate states between the silent state

*E-mail: wclim@kangwon.ac.kr
†Corresponding Author; E-mail: sykim@kangwon.ac.kr

and the chaotic bursting state. Using a rational approximation to quasiperiodic forcing [13, 14], we investigate the mechanism for the appearance of such SN burstings. Thus, a smooth torus, corresponding to a silent state, is found to transform to an SN bursting attractor via a phase-dependent subcritical period-doubling bifurcation. Together with chaotic burstings, these SN burstings are characterized in terms of the interburst interval, the bursting length, and the number of spikes in each burst. Both the chaotic and the SN bursting states are found to be aperiodic complex ones. Such aperiodic complexity comes from the strange geometry of both bursting states with qualitatively different dynamics (one is chaotic, and the other one is nonchaotic). We note that complex physiological rhythms, which are central to life, are ubiquitous in organisms [6]. Hence, in addition to chaotic burstings, SN burstings may also serve as a dynamical origin of such complex bodily rhythms. Finally, a summary is given in Sec. III.

II. SN BURSTINGS IN THE QUASIPERIODICALLY-FORCED HR NEURON

We consider a representative HR bursting neuron model [9,15,16], which is quasiperiodically forced at two incommensurate frequencies f_1 and f_2:

$$\frac{dx}{dt} = y - ax^3 + bx^2 - z + I_{\text{ext}}, \tag{1a}$$

$$\frac{dy}{dt} = c - dx^2 - y, \tag{1b}$$

$$\frac{dz}{dt} = r[s(x - x_0) - z], \tag{1c}$$

where $I_{\text{ext}} = I_{\text{dc}} + A_1 \sin(2\pi f_1 t) + A_2 \sin(2\pi f_2 t)$, $a = 1$, $b = 3$, $c = 1$, $d = 5$, $s = 1$, $r = 0.001$, and $x_0 = -1.6$. Here, t is the time [measured in units of millisecond (ms)], x is the membrane potential variable, y is the recovery variable, z is the slow adaptation current, I_{dc} is a dc stimulus, A_1 and A_2 are amplitudes of quasiperiodic forcing, and ω ($\equiv f_2/f_1$) is irrational (f_1 and f_2 are measured in units of kHz).

To obtain the Poincaré map of Eq. (1), we make a normalization $f_1 t \rightarrow t$, then, Eq. (1) can be reduced to the following differential equations:

$$\frac{dx}{dt} = F_1(\mathbf{x}, \theta) = \frac{1}{f_1}(y - ax^3 + bx^2 - z + I_{\text{ext}}), \tag{2a}$$

$$\frac{dy}{dt} = F_2(\mathbf{x}, \theta) = \frac{1}{f_1}(c - dx^2 - y), \tag{2b}$$

$$\frac{dz}{dt} = F_3(\mathbf{x}, \theta) = \frac{r}{f_1}[s(x - x_0) - z], \tag{2c}$$

$$\frac{d\theta}{dt} = \omega \pmod 1, \tag{2d}$$

where $\mathbf{x} = (x, y, z)$ and $I_{\text{ext}} = I_{\text{dc}} + A_1 \sin(2\pi t) + A_2 \sin(2\pi\theta)$. The phase space of the quasiperiodically-forced HR oscillator is five dimensional with coordinates x, y, z, θ, and t. Since the system is periodic in θ and t, they are circular coordinates in the phase space. Then, we consider the surface of section, the x-y-z-θ hypersurface at $t = n$ (n: integer). The phase-space trajectory intersects the surface of section in a sequence of points. This sequence of points corresponds to a mapping on the four-dimensional hypersurface. The map can be computed by stroboscopically sampling the orbit points $\mathbf{v}_n$ [$\equiv (\mathbf{x}_n, \theta_n)$] at the discrete time n (corresponding to multiples of the first external driving period T_1). We call the transformation $\mathbf{v}_n \rightarrow \mathbf{v}_{n+1}$ the Poincaré map and write $\mathbf{v}_{n+1} = P(\mathbf{v}_n)$.

Numerical integration of Eqs. (1) and (2) is done using the fourth-order Runge-Kutta method. A dynamical analysis is performed in both the continuous-time system (i.e., flow) and the discrete-time system (i.e., Poincaré map). For example, the time series of the membrane potential $x(t)$, the phase flow, the interburst interval, the bursting length, and the average number of spikes per burst are obtained in the flow. On the other hand, the Lyapunov exponent [17] and the phase sensitivity exponent [13] of an attractor are calculated in the Poincaré map. To obtain the Lyapunov exponent of an attractor in the Poincaré map, we choose 20 random initial points $\{(x_i(0), y_i(0), z_i(0), \theta_i(0)); i = 1, \ldots, 20\}$ with uniform probability in the range of $x_i(0) \in (-2, 2)$, $y_i(0) \in (-16, 0)$, $z_i(0) \in (0, 0.4)$, and $\theta_i(0) \in [0, 1)$. For each initial point, we get the Lyapunov exponent [17] and choose the average value of the 20 Lyapunov exponents. (The method of obtaining the phase-sensitivity exponent will be explained below.)

Here, we set ω to be the reciprocal of the golden mean [i.e., $\omega = (\sqrt{5} - 1)/2$] and numerically investigate the dynamical transition from a silent state to a bursting state by varying I_{dc} in the HR neuron under an external stimulus. We first consider the case of periodic forcing (i.e., $A_2 = 0$) for $A_1 = 0.5$ and $f_1 = 30$ Hz. Figures 1(a) and 1(b) show the time series of $x(t)$ and the projection of the phase flow onto the x-z plane for the silent state when $I_{dc} = 0.3$. We note that this silent state with the largest Lyapunov exponent $\sigma_1 \simeq -0.133$ exhibits sub-threshold oscillations. As I_{dc} passes a threshold value of $I_{dc} = 0.416\,721$, a chaotic bursting state appears. Bursting activity [alternating between a silent phase and an active (bursting) phase of repetitive spikings] of the HR neuron is shown in Fig. 1(c) for $I_{dc} = 0.5$. This kind of bursting occurs on a chaotic hedgehoglike attractor with $\sigma_1 \simeq 0.406$ [the body (spines) of the hedgehoglike attractor corresponds to the silent (bursting) phase], as shown in Fig. 1(d). This transition from a silent state to a chaotic bursting state is investigated by varying I_{dc} in the Poincaré map. Figure 1(e) shows the bifurcation diagram (i.e., plot of x versus I_{dc}). The solid curve represents a stable fixed point corresponding to the silent state. The stable fixed point loses its stability for
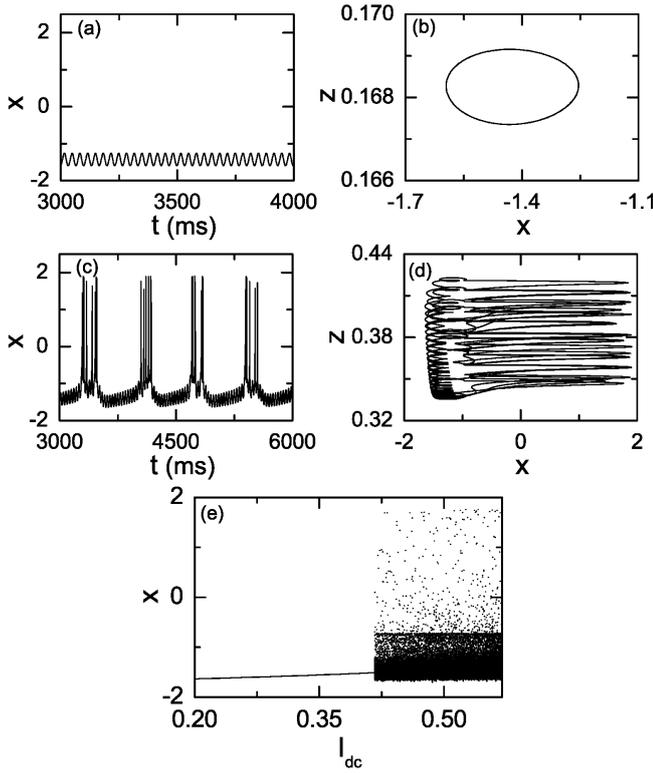
Fig. 1. Intermittent transition to a chaotic bursting state for the case of periodic forcing with $A_1 = 0.5$ and $f_1 = 30$ Hz ($A_2 = 0$). (a) Time series of $x(t)$ and (b) projection of the phase flow onto the $x - z$ plane for the silent state exhibiting subthreshold oscillations for $I_{dc} = 0.3$. (c) Time series of $x(t)$ and (d) projection of the phase flow onto the $x - z$ plane for the chaotic bursting state for $I_{dc} = 0.5$. (e) Bifurcation diagram (*i.e.*, plot of x versus I_{dc}) in the Poincaré map. We obtain attractors by iterating the Poincaré map at the 500 equally-spaced values of I_{dc} in the range of $I_{dc} \in [0.2, 0.57]$. For each chosen I_{dc}, we choose a random initial point $(x(0), y(0), z(0), \theta(0))$ with uniform probability in the ranges $x(0) \in (-2, 2)$, $y(0) \in (-16, 0)$, $z(0) \in (0, 0.4)$, and $\theta(0) \in [0, 1)$ and obtain the attractor through the 200-times iterations of the Poincaré map after the transients of the 1000 Poincaré maps.

$I_{dc} = 0.416\,721$ via a subcritical Hopf bifurcation when a pair of complex conjugate stability multipliers passes the unit circle in the complex plane; then, a chaotic bursting attractor, corresponding to a chaotic bursting state, appears.

From now on, we consider the quasiperiodically-forced case for $A_1 = 0.5$ and $f_1 = 30$ Hz. Each state is characterized by both the largest (nontrivial) Lyapunov exponent σ_1, associated with dynamics of the variable **x** [besides the (trivial) zero exponent, related to the phase variable θ of the quasiperiodic forcing] and the phase sensitivity exponent δ. The exponent δ measures the sensitivity of the variable **x** with respect to the phase θ of the quasiperiodic forcing and characterizes the strangeness of an attractor [13]. A (regular) silent state has a nega-
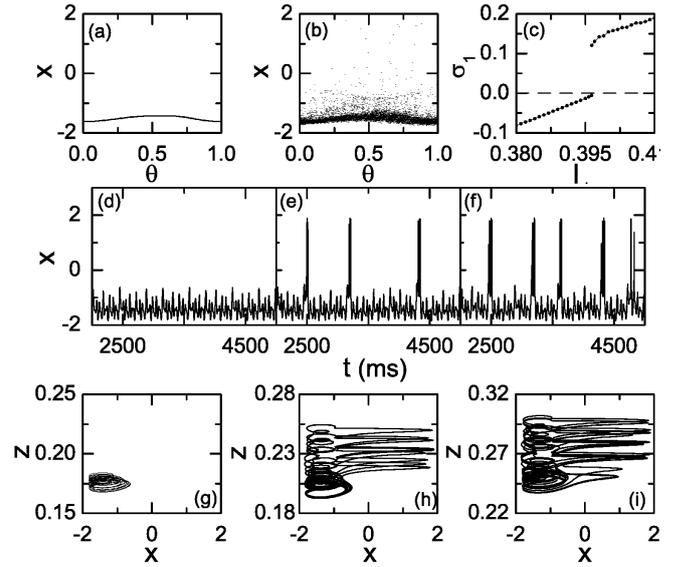

Fig. 2. Transition from a silent state to a bursting state for the quasiperiodically-forced case when $A_1 = 0.5$ and $f_1 = 30$ Hz. We set $A_2 = 0.2$ in (a) - (c). Projections of attractors onto the $\theta - x$ plane in the Poincaré map are shown for (a) the silent and (b) the chaotic bursting states when $I_{dc} = 0.39$, and 0.4. (c) Lyapunov-exponent diagram (*i.e.*, plot of σ_1 versus I_{dc}). For each randomly chosen initial point, we get the Lyapunov exponent by following the 10^4 Poincaré maps after the transients of the 10^4 Poincaré maps. We set $A_2 = 0.5$ for (d) - (i). Time series of $x(t)$ of (d) the silent state for $I_{dc} = 0.21$, (e) the SN bursting state for $I_{dc} = 0.24$, and (f) the chaotic bursting state for $I_{dc} = 0.29$. Projections of the phase flows onto the $x - z$ plane for (g) the silent state for $I_{dc} = 0.21$, (h) the SN bursting state for $I_{dc} = 0.24$, and (i) the chaotic bursting state for $I_{dc} = 0.29$.

tive Lyapunov exponent (*i.e.*, $\sigma_1 < 0$) and has no phase sensitivity (*i.e.*, $\delta = 0$). On the other hand, a chaotic bursting state has a positive Lyapunov exponent $\sigma_1 > 0$. In addition to them, new types of SN bursting states that have negative Lyapunov exponents ($\sigma_1 < 0$) and positive phase sensitivity exponents ($\delta > 0$) appear. Due to their high phase sensitivity, SN bursting states have a strange fractal phase space structure. For small A_2, a direct transition from a silent state to a chaotic bursting state occurs, as in the periodically-forced case of $A_2 = 0$. As an example, we consider the case of $A_2 = 0.2$ where a transition to chaotic bursting occurs for $I_{dc} = 0.3963$. Figures 2(a) and 2(b) show a smooth torus with $\sigma_1 \simeq -0.036$ (corresponding to a silent state) and a chaotic bursting attractor with $\sigma_1 \simeq 0.154$ (corresponding to a chaotic bursting state) for $I_{dc} = 0.39$ and 0.4, respectively. Figure 2(c) shows the Lyapunov-exponent diagram (*i.e.*, plot of σ_1 *vs.* I_{dc}). As I_{dc} is increased to the transition point, σ_1 of the smooth torus increases to zero; then, a chaotic bursting attractor with a (finite) positive σ_1 appears (*i.e.*, a finite jump for the value of σ_1 seems to occur). However, for A_2 larger than a threshold A_2^* (~ 0.4), SN bursting states appear between the silent and the
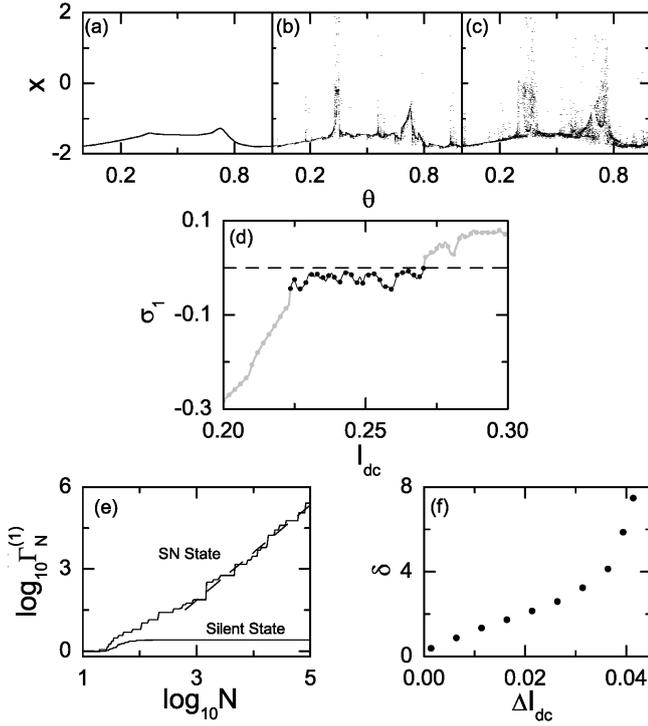
Fig. 3. Characterization of silent and bursting states for $A_1 = 0.5$, $A_2 = 0.5$, and and $f_1 = 30$ Hz. Projections of attractors onto the $\theta - x$ plane in the Poincaré map are shown for the (a) silent, (b) SN bursting, and (c) chaotic bursting states when $I_{dc} = 0.21$, 0.24, and 0.29. (d) Lyapunov-exponent diagram (i.e., plot of σ_1 versus I_{dc}); σ_1 for the SN bursting attractor is shown in black. For each randomly chosen initial point, we get the Lyapunov exponent by following the 10^4 Poincaré maps after the transients of the 10^3 Poincaré maps. (e) Phase sensitivity functions $\Gamma_N^{(1)}$ are shown for the silent and the SN bursting attractors when $I_{dc} = 0.21$ and 0.24. For the case of the SN bursting attractor, the graph is well fitted with a dashed straight line with slope $\delta \simeq 1.74$. (f) Plot of the phase sensitivity exponent δ versus ΔI_{dc} ($= I_{dc} - I_{dc}^*$) for the SN bursting attractor; $I_{dc}^* \simeq 0.2236$.

chaotic bursting states. As an example, we consider the case of $A_2 = 0.5$ and investigate the dynamical behaviors of a quasiperiodically-forced HR neuron by varying I_{dc}. As I_{dc} passes a threshold I_{dc}^* ($\simeq 0.2236$), the silent state becomes unstable, and a transition to an SN bursting state occurs. As I_{dc} is increased further and passes another threshold value of $I_{dc} \simeq 0.2703$, the SN bursting state transforms to a chaotic bursting state. Figures 2(d) - 2(f) show the time series of the membrane potential $x(t)$ of a silent state (exhibiting subthreshold oscillations), an SN bursting state, and a chaotic bursting state for $I_{dc} = 0.21$, 0.24, and 0.29, respectively. For these three cases, the phase flows of the silent, SN bursting and chaotic bursting states are also given in Figs. 2(g) - 2(i), respectively.

The silent and the bursting states for $A_2 = 0.5$ are analyzed in terms of the largest Lyapunov exponent σ_1 and the phase sensitivity exponent δ in the Poincaré map.

Projections of the attractors onto the $\theta - x$ plane for $I_{dc} = 0.21$, 0.24, and 0.29 are given in Figs. 3(a) - 3(c), respectively. For the silent case, a smooth torus exists in the $\theta - x$ plane [see Fig. 3(a)]. On the other hand, nonsmooth bursting attractors appear for both SN and chaotic bursting states, as shown in Figs. 3(b) and 3(c). The dynamical property of each state is characterized in terms of the largest Lyapunov exponent σ_1 (measuring the degree of sensitivity to the initial conditions). The Lyapunov-exponent diagram is given in Fig. 3(d). When passing the bursting transition point I_{dc}^* ($\simeq 0.2236$), an SN bursting attractor appears. The graph of σ_1 for the SN bursting state is shown in black; it is nearly flat, and its value is negative as in the case of a smooth torus. However, as I_{dc} passes the chaotic transition point I_{dc} ($\simeq 0.2703$), a chaotic bursting attractor with a positive σ_1 appears. Unlike the case of a direct transition from a smooth torus to a chaotic bursting attractor, σ_1 seems to increase continuously from zero without a jump [compare Fig. 3(d) with Fig. 2(c)]. Although SN and chaotic bursting attractors are dynamically different, they both have strange geometry, leading to aperiodic complex burstings. To characterize the strangeness of an attractor, we investigate the sensitivity of the attractor with respect to the phase θ of the external quasiperiodic forcing [13]. This phase sensitivity may be characterized by differentiating $\mathbf{x}$ with respect to θ at a discrete time $t = n$. Using Eq. (2), we may obtain the following governing equation for $\frac{\partial x_i}{\partial \theta}$ ($i = 1, 2, 3$):

$$\frac{d}{dt}\left(\frac{\partial x_i}{\partial \theta}\right) = \sum_{j=1}^{3} \frac{\partial F_i}{\partial x_j} \cdot \frac{\partial x_j}{\partial \theta} + \frac{\partial F_i}{\partial \theta}, \qquad (3)$$

where $(x_1, x_2, x_3) = (x, y, z)$ and F_i's ($i = 1, 2, 3$) are given in Eq. (2). Starting from an initial point $(\mathbf{x}(0), \theta(0))$ and an initial value $\partial \mathbf{x}/\partial \theta = \mathbf{0}$ for $t = 0$, we may obtain the derivative values of $S_n^{(i)}$ ($\equiv \partial x_i/\partial \theta$) at all subsequent discrete time $t = n$ by integrating Eqs. (2) and (3). One can easily see the boundedness of $S_n^{(i)}$ by looking only at the maximum

$$\gamma_N^{(i)}(\mathbf{x}(0), \theta(0)) = \max_{0 \le n \le N} |S_n^{(i)}(\mathbf{x}(0), \theta(0))| \;\; (i = 1, 2, 3).$$
$$(4)$$

We note that $\gamma_N^{(i)}(\mathbf{x}(0), \theta(0))$ depends on a particular trajectory. To obtain a "representative" quantity that is independent of a particular trajectory, we consider an ensemble of randomly chosen initial points $\{(\mathbf{x}(0), \theta(0))\}$ and take the minimum value of $\gamma_N^{(i)}$ with respect to the initial orbit points [13]:

$$\Gamma_N^{(i)} = \min_{\{(\mathbf{x}(0), \theta(0))\}} \gamma_N^{(i)}(\mathbf{x}(0), \theta(0)) \;\; (i = 1, 2, 3). \quad (5)$$

Figure 3(e) shows a phase sensitivity function $\Gamma_N^{(1)}$, which is obtained in an ensemble containing 20 random initial

orbit points $\{(x_i(0), y_i(0), z_i(0), \theta_i(0)); \; i = 1, \ldots, 20\}$ chosen with uniform probability in the range of $x_i(0) \in (-2, 2)$, $y_i(0) \in (-16, 0)$, $z_i(0) \in (0, 0.4)$, and $\theta_i(0) \in [0, 1)$. For the silent case of $I_{dc} = 0.21$, $\Gamma_N^{(1)}$ grows up to the largest possible value of the derivative $|\partial x_1/\partial \theta|$ along a trajectory and remains there for all subsequent time. Thus, $\Gamma_N^{(1)}$ saturates for large N, hence, the silent state has no phase sensitivity (*i.e.*, it has smooth geometry). On the other hand, for the case of SN bursting, $\Gamma_N^{(i)}$ grows unboundedly with the same power δ, independently of i,

$$\Gamma_N^{(i)} \sim N^\delta. \tag{6}$$

Here, the value of $\delta \simeq 1.74$ is a quantitative characteristic of the phase sensitivity of the SN bursting attractor for $I_{dc} = 0.24$, and δ is called the phase sensitivity exponent. To obtain satisfactory statistics, we consider 20 ensembles for each I_{dc}, each of which contains 20 randomly chosen initial points, and we take the average value of the 20 phase sensitivity exponents obtained in the 20 ensembles. Figure 3(f) shows a plot of δ versus ΔI_{dc} ($= I_{dc} - I_{dc}^*$). Note that the value of δ monotonically increases from zero as I_{dc} is increased away from the bursting transition point I_{dc}^* ($\simeq 0.2236$). As a result of this phase sensitivity, the SN bursting attractor has strange geometry leading to aperiodic complex bursting, as in the case of chaotic bursting attractor.

Using the rational approximation to quasiperiodic forcing [13,14], we explain the mechanism for the transition from a silent to an SN bursting state. For the inverse golden mean, its rational approximants are given by the ratios of the Fibonacci numbers, $\omega_k = F_{k-1}/F_k$, where the sequence of $\{F_k\}$ satisfies $F_{k+1} = F_k + F_{k-1}$ with $F_0 = 0$ and $F_1 = 1$. Instead of the quasiperiodically-forced system, we study an infinite sequence of periodically-forced systems with rational driving frequencies ω_k. For each rational approximation of level k, a periodically-forced system has a periodic or a chaotic attractor that depends on the initial phase θ_0 of the external forcing. Then, the union of all attractors for different θ_0 gives the kth approximation to the attractor in the quasiperiodically-forced system. For this rational approximation of level k, it is sufficient to change the initial phase θ_0 in the interval $[0, 1/F_k)$ in order to get all possible attracting sets, because the set of all θ values fills the whole interval $[0, 1)$.

We consider the rational approximation of level $k = 7$ to the quasiperiodic forcing of $A_2 = 0.5$. As shown in Fig. 4(a) for $I_{dc} = 0.22$, the rational approximation to a stable smooth torus (represented by the black curve), corresponding to a silent state, consists of stable orbits with period F_7 ($=13$). Figure 4(b) shows the magnitude of the first stability multiplier λ_1 (with the largest magnitude) of the stable F_7-periodic orbits in the interval $[0, 1/F_7)$. We note that $|\lambda_1|$ varies depending on θ and that all of its values are less than unity. Hence, all F_7-periodic orbits for all θ are stable. However, as I_{dc} passes a threshold value $I_{dc,7}$ ($\simeq 0.2209$), the smooth torus be-
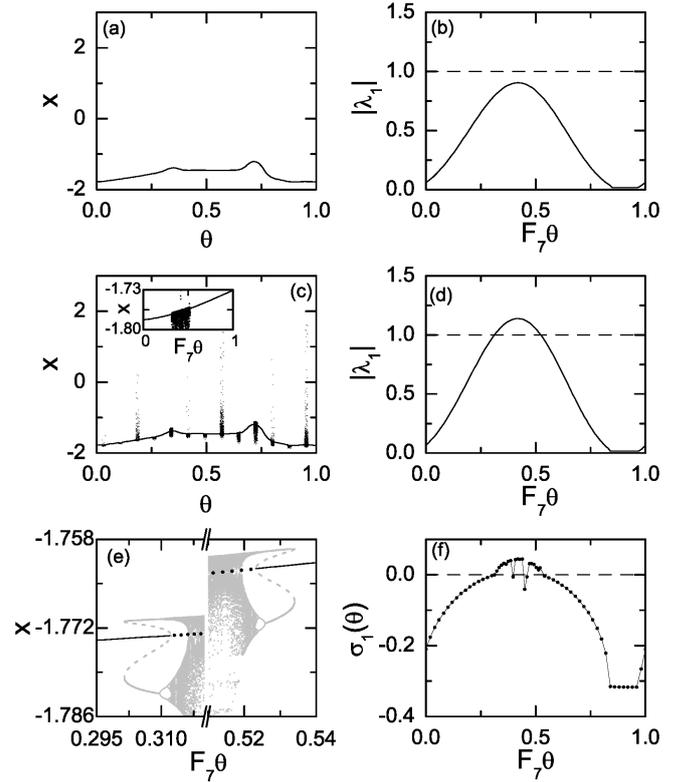

Fig. 4. Investigation of the transition from a smooth torus (corresponding to a silent state) to an SN bursting attractor (corresponding to an SN bursting state) in the rational approximation of level $k = 7$ for $A_1 = 0.5$, $A_2 = 0.5$, and $f_1 = 30$ Hz. In (a) and (c), projections of attractors onto the θ-x plane are given. (a) Stable smooth torus corresponding to the silent state for $I_{dc} = 0.22$. (b) Plot of $|\lambda_1|$ *vs.* $F_7\theta$ for $I_{dc} = 0.22$ [λ_1: the first stability multiplier (with largest magnitude) of the F_7-periodic orbit]. (c) SN bursting attractor for $I_{dc} = 0.222$. A magnified view of the 1st gap is also given in the inset. (d) Plot of $|\lambda_1|$ *vs.* $F_7\theta$ for $I_{dc} = 0.222$. (e) Bifurcation diagram (*i.e.*, plot of x *vs.* $F_7\theta$) for $I_{dc} = 0.222$ in the F_7-times iterated Poincaré map P^{F_7}. An F_7-periodic orbit (represented by a black solid line) becomes unstable via a subcritical period-doubling bifurcation; then, it is denoted by solid black circles. (f) Lyapunov-exponent diagram for $I_{dc} = 0.222$ in the Poincaré map. For each randomly chosen initial point, we get the Lyapunov exponent by following the 10^4 Poincaré maps after the transients of the 10^3 Poincaré maps.

comes broken, and a nonsmooth bursting attracting set with F_7 "gaps", where no stable orbits with period F_7 exist, appears. An example is given in Fig. 4(c) for $I_{dc} = 0.222$. A magnified view of the 1st gap is given in the inset. For this case, Fig. 4(d) shows $|\lambda_1|$ of the F_7-periodic orbits in the interval $[0, 1/F_7)$. In the gap where $0.312\,306 < F_7\theta < 0.523\,202$, $|\lambda_1|$ is larger than unity, while in the remaining region of θ, $|\lambda_1|$ is less than unity. Thus, the F_7-periodic orbits in the gap become unstable via phase-dependent bifurcations (occurring at specific values of θ); then, chaotic bursting attractors fill the gap

together with regular attractors with periods higher than F_7 embedded in small windows. The bifurcation diagram (*i.e.*, plot of x *vs.* $F_7\theta$ in the F_7-times iterated Poincaré map P^{F_7}) for $I_{\rm dc} = 0.222$ is given in Fig. 4(e). At both ends of the gap, the F_7-periodic attractor (denoted by the black solid curve) becomes unstable via a subcritical period-doubling bifurcation when it absorbs an unstable orbit with doubled period $2F_7$ (represented by the gray short-dashed curve). Then, a jump to a chaotic bursting attractor [developed from the period-doubling cascade of the stable $2F_7$-periodic orbit (denoted by the gray solid curve)] occurs. Thus, in Fig. 4(c), the rational approximation to the whole attractor consists of the union of the periodic component and the chaotic bursting component, where the latter occupies F_7 gaps in θ. Figure 4(f) shows the Lyapunov-exponent diagram (*i.e.*, plot of $\sigma_1(\theta)$ *vs.* $F_7\theta$) for $I_{\rm dc} = 0.222$. (In the gap, chaotic bursting attractors with positive σ_1 coexist with periodic attractors with negative σ_1 embedded in small windows.) The angle-averaged Lyapunov exponent $\langle\sigma_1\rangle$ [$\langle\cdots\rangle$ denotes the average over all θ] is given by the sum of the "weighted" Lyapunov exponents of the periodic and the chaotic components, Λ_p and Λ_c, (*i.e.*, $\langle\sigma_1\rangle = \Lambda_p + \Lambda_c$), where $\Lambda_{p(c)} = M_{p(c)}\langle\sigma_1\rangle_{p(c)}$, and $M_{p(c)}$ and $\langle\sigma_1\rangle_{p(c)}$ are the Lebesgue measure in θ and the average Lyapunov exponent of the periodic (chaotic) component, respectively. Since the periodic component is dominant, the average Lyapunov exponent ($\langle\sigma_1\rangle \simeq -0.073$) is negative. Hence, the rational approximation to the whole attractor in Fig. 4(c) is nonchaotic. We note that Fig. 4(c) resembles Fig. 3(b), although the level $k = 7$ is low. Increasing the level to $k = 10$, we confirm that the rational approximations to the whole attractor have F_k gaps (filled with chaotic bursting attractors) which appear via phase-dependent subcritical period-doubling bifurcations, and that their average Lyapunov exponents are negative. In this way, a SN bursting attractor appears in the case of quasiperiodic forcing, as shown in Fig. 3(b).

Finally, we characterize the bursting activity [alternating between the silent phase and the active (bursting) phase] in both cases of SN and chaotic bursting states for $A_2 = 0.5$. Figures 5(a1) and 5(a2) show sequences of the interburst intervals [*i.e.*, time interval between the first spikes in the neighboring bursts (*i.e.*, active phases)] for the SN and the chaotic bursting states when $I_{dc} = 0.24$ and 0.29, respectively. Both sequences are aperiodic complex ones. Histograms of the interburst intervals for these SN and chaotic bursting states are also given in Figs. 5(b1) and 5(b2), respectively. They are multimodal ones. As $I_{\rm dc}$ is increased, the heights of the peaks for short interburst intervals increase while those for longer ones decrease. Hence, as $I_{\rm dc}$ is increased, the average interburst interval $\langle\text{IBI}\rangle$ ($\langle\cdots\rangle$ represents the average over a large number of bursts) decreases (*i.e.*, the mean bursting rate increases); $\langle\text{IBI}\rangle \simeq 1029$ ms and 549 ms for $I_{dc} = 0.24$ and 0.29, respectively. The active (bursting) phases are also characterized in terms of the bursting length (BL) (*i.e.*, time interval between the first
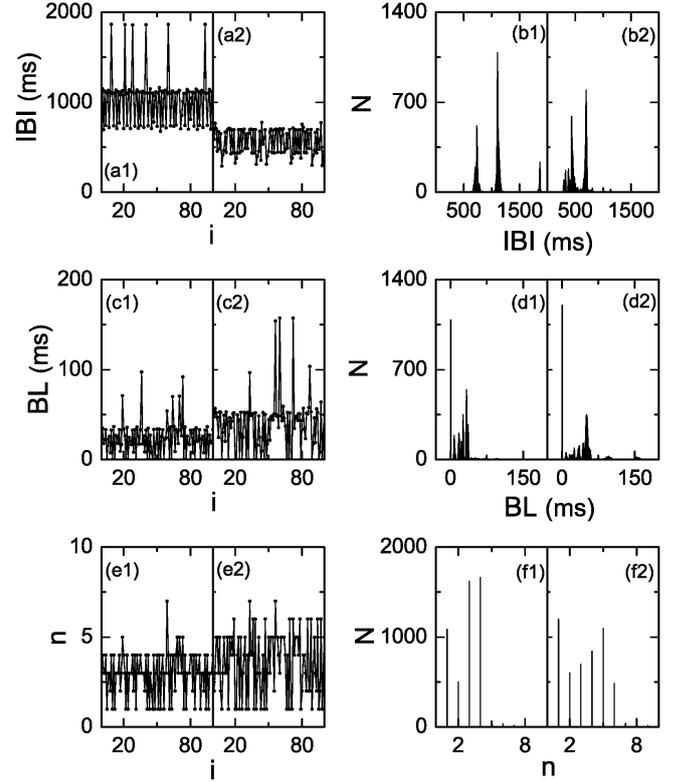

Fig. 5. Characterization of SN ($I_{\rm dc} = 0.24$) and chaotic ($I_{\rm dc} = 0.29$) bursting states for $A_1 = 0.5$, $A_2 = 0.5$, and $f_1 = 30$ Hz. Sequences of interburst intervals (IBIs) for (a1) SN and (a2) chaotic burstings; i represents the bursting index. Histograms of IBIs for (b1) SN and (b2) chaotic burstings. Sequences of bursting length (BL) for (c1) SN and (c2) chaotic burstings. Histograms of BL for (d1) SN and (d2) chaotic burstings. Sequences of number of spikes (n) per burst for (e1) SN and (e2) chaotic burstings. Histograms of n for (f1) SN and (f2) chaotic burstings. For histograms of IBI and BL, 200 equally-spaced bins are chosen in the range of IBI $\in (0, 2000)$ and BL $\in (0, 200)$. We get the number of bursts (N) in each bin among total number of 5000 bursts (which are also used for the histogram of n).

and the last spikes in a burst) and the number of spikes (n) per burst. For our cases of SN and weakly chaotic burstings, some of the active phases are found to consist of only one spike (*i.e.*, n = 1); hence, their BLs are zero. The presence of these active phases with n = 1 implies "weak" firing activity in such active phases. (This is in contrast to the periodically-forced case (of $A_2 = 0$) where a direct transition from a silent to a chaotic bursting state with all active phases composed of more than one spike occurs.) Sequences of both BL and n are shown in Figs. 5(c1) - 5(c2) and Figs. 5(e1) - 5(e2). As in the case of the interburst intervals, they are aperiodic and complex for both the SN and the chaotic burstings. Likewise, their histograms are also multimodal, as shown in Figs. 5(d1) - 5(d2) and Figs. 5(f1) - 5(f2). With increasing $I_{\rm dc}$, both the average bursting length $\langle\text{BL}\rangle$ and the average number of spikes $\langle n\rangle$ in a burst increase; $\langle\text{BL}\rangle \simeq 23$ ms

and 39 ms, and $\langle n \rangle \simeq 2.9$ and 3.4 for $I_{dc} = 0.24$ and 0.29, respectively. Thus, both the SN and the chaotic bursting states exhibit aperiodic complex burstings, although their dynamics are different (one is chaotic, and the other is nonchaotic). We note that such aperiodic complexity results from the strange geometry of the SN and the chaotic bursting states.

III. SUMMARY

We have investigated a dynamical transition from a silent state to a bursting state by varying the dc stimulus, I_{dc}, in the quasiperiodically-forced HR neuron. For this case of quasiperiodic forcing, a transition from a silent state to an SN bursting state (with negative Lyapunov exponent and positive phase sensitivity exponent) has been found to occur when I_{dc} passes a threshold value. With further increase in I_{dc}, such an SN bursting state transforms to a chaotic bursting state (with a positive Lyapunov exponent). Thus, a new type of SN bursting state appears as an intermediate state between the silent and the chaotic bursting states. This is in contrast to the periodically-forced case where a direct transition from a silent state to a chaotic bursting state occurs. Using a rational approximation to quasiperiodic forcing, we have studied the mechanism for the appearance of SN bursting states. Thus, a smooth torus, corresponding to a silent state, is found to transform to an SN bursting attractor through a phase-dependent subcritical period-doubling bifurcation. Both the SN and the chaotic bursting states have been characterized in terms of the interburst intervals, the bursting lengths, and the number of spikes per burst. As a result of their strange geometry, both bursting states are found to be aperiodic complex ones, although their dynamics are qualitatively different. Hence, we note that not only chaotic but also SN burstings may become the dynamical origin of the complex physiological rhythms that are central to life and ubiquitous in organisms.

ACKNOWLEDGMENTS

REFERENCES

[1] M. R. Guevara, L. Glass and A. Shrier, Science **214**, 1350 (1981); L. Glass, M. R. Guevara, A. Shrier and R. Perez, Physica D **7**, 89 (1983).

[2] K. Aihara, T. Numajiri, G. Matsumoto and M. Kotani, Phys. Lett. A **116**, 313 (1986); N. Takahashi, Y. Hanyu, T. Musha, R. Kubo and G. Matsumoto, Physica D **43**, 318 (1990); D. T. Kaplan, J. R. Clay, T. Manning, L. Glass, M. R. Guevara and A. Shrier, Phys. Rev. Lett. **76**, 4074 (1996).

[3] K. Aihara, Scholarpedia **3**, 1786 (2008) and references therein.

[4] R. Stoop, K. Schindler and L. A. Bunimovich, Neurosci. Res. **36**, 81 (2000); Nonlinearity **13**, 1515 (2000).

[5] L. Glass and M. C. Mackey, *From Clocks to Chaos* (Princeton University Press, Princeton, 1988).

[6] L. Glass, Nature **410**, 277 (2001).

[7] M. Ding and J. A. S. Kelso, Int. J. Bifurcation Chaos Appl. Sci. Eng. **4**, 553 (1994).

[8] W. Lim, S.-Y. Kim and Y. Kim, Prog. Theor. Phys. **121**, 671 (2009); W. Lim and S.-Y. Kim, J. Phys. A **42**, 265103 (2009); J. Korean Phys. Soc. **57**, 23 (2010).

[9] *Bursting: The Genesis of Rhythm in the Nervous System*, edited by S. Coombes and P. C. Bressloff (World Scientific, Singapore, 2005).

[10] E. M. Izhikevich, *Dynamical Systems in Neuroscience* (MIT Press, Cambridge, 2007), p. 325.

[11] C. Grebogi, E. Ott, S. Pelikan and J. A. Yorke, Physica D **13**, 261 (1984).

[12] U. Feudel, S. Kuznetsov and A. Pikovsky, *Strange Nonchaotic Attractors* (World Scientific, Singapore, 2006) and references therein.

[13] A. S. Pikovsky and U. Feudel, Chaos **5**, 253 (1995).

[14] S.-Y. Kim, W. Lim and E. Ott, Phys. Rev. E **67**, 056203 (2003); S.-Y. Kim and W. Lim, J. Phys. A **37**, 6477 (2004); Phys. Lett. A **334**, 160 (2005); W. Lim and S.-Y. Kim, *ibid.* **335**, 383 (2005); *ibid.* **355**, 331 (2006); J.-W. Kim, S.-Y. Kim, B. Hunt and E. Ott, Phys. Rev. E **67**, 036211 (2003).

[15] J. L. Hindmarsh and R. M. Rose, Nature **296**, 162 (1982); Proc. R. Soc. London, Ser. B **221**, 87 (1984); **225**, 161 (1985).

[16] G. Innocenti and R. Genesio, Chaos **19**, 023124 (2009); G. Innocenti, A. Morelli, R. Genesio and A. Torcini, Chaos **17**, 043128 (2007).

[17] A. J. Lichtenberg and M. A. Lieberman, *Regular and Stochastic Motion* (Springer-Verlag, New York, 1983), p. 283; A. Wolf, J. B. Swift, H. L. Swinney and J. A. Vastano, Physica D **16**, 285 (1985).